JMEPEG
https://doi.org/10.1007/s11665-024-09999-y

1059-9495/$19.00

ORIGINAL RESEARCH ARTICLE

Effects of Ta Addition on the Microstructure, Compression Properties and Oxidation Resistance of NiAl-Cr(Mo) Alloy

Zhao Shang, Tian Liu, Jun Shen, Wenfang Bai, Xiaowan Dong, and Jungang Yang

Submitted: 17 May 2024 / Revised: 08 July 2024 / Accepted: 26 July 2024

The effects of Ta addition on the microstructure, compression properties and oxidation resistance of NiAl-32Cr-6Mo alloy were investigated. The microstructure of NiAl-32Cr-6Mo hypereutectic alloy comprises Cr(Mo) primary dendrites and NiAl + Cr(Mo) eutectic. After Ta addition, Cr_2Ta phase, NiAl + Cr(Mo) two-phase eutectic and NiAl + Cr(Mo) + Cr_2Ta three-phase eutectic are observed. Increasing Ta content changes the primary phase from Cr(Mo) to Cr_2Ta, disrupts the formation of eutectic lamellae and degrades the eutectic cell. Ta addition leads to a decreasing room-temperature compression strength but a significantly increasing high-temperature compression strength. At 1000 °C, NiAl-Cr(Mo)-6Ta alloy has a compression strength of 475.1 MPa, which is about nine times than that of binary NiAl alloy and two times than that of NiAl-Cr(Mo) alloy. Room-temperature fractures present brittle pseudo-cleavage with tearing edges and cleavage steps, while high-temperature fractures indicate typically plastic deformation. Cracks in alloys containing Ta no longer propagate along the interfaces between eutectic cells or between the primary phase and eutectic. Improved high-temperature strength of Ta-added alloys results from precipitation strengthening of Cr_2Ta, solid solution strengthening of Ta and strong interface. Furthermore, Ta addition obviously enhances the oxidation resistance of NiAl-Cr(Mo) alloy, especially at higher temperature.

Keywords compression properties, fractography, intermetallic alloys, microstructure, oxidation resistance, Ta addition

1. Introduction

High-temperature structural materials with higher specific strength and temperature resistance are urgently needed due to the rapid development in the fields of aerospace and energy (Ref 1-3). Currently, Ni-based single crystal superalloys are widely used to prepare hot ends in aeroengines, but further increasing its service temperature is difficult (Ref 4). The B2 structure intermetallic NiAl compounds has attracted wide attention because of its many advantages, such as high specific strength, high melting point, low density, higher Young's modulus and thermal conductivity as well as excellent resistance to oxidation and corrosion at high temperature, which make it potential application prospects for advanced aeroengines (Ref 5-8). However, the actual application of NiAl is constrained by insufficient high-temperature strength and poor room-temperature ductility (Ref 9). To improve the comprehensive properties of NiAl, several strengthening methods, such as mechanical alloying, fine grain toughening, ductile phase toughening, heat treatment, preparation of composite materials, introducing multiscale high-entropy phases and martensitic transformation, were proposed (Ref 5-18). For example, the room-temperature fracture toughness and high-temperature tensile strength could be simultaneously improved by adding varying amounts of Cr and Mo elements resulting from the existence of Cr(Mo) strengthening phase in the NiAl-Cr(Mo) composites (Ref 11, 12).

However, the high-temperature strength of NiAl-Cr(Mo) composites is still inferior to that of Ni-based single crystal superalloys. To further increase the high-temperature strength, Wang et al. prepared NiAl-based alloy with a Cr(Mo) reinforced bipolar network by rapid solidification and hot pressing sintering, which significantly improved the high-temperature strength of alloy (Ref 13). Furthermore, different contents of alloying elements such as Fe, Ti, Nb, Hf, V, Zr, Ho and Ta were added to the NiAl-Cr(Mo) alloy to enhance the high-temperature strength by solid solution strengthening and precipitation strengthening (Ref 4, 8, 14-19). In the previous work of Shang et al., the compression strength of NiAl-32Cr-6Mo-1Ti reached 409 MPa at 1000 °C due to the strengthening effect of the Ni_2AlTi phase (Ref 17). In addition, the addition of Hf could also improve the high-temperature strength of NiAl-Cr(Mo) alloy, but the room-temperature brittleness and little compression strain were still not improved (Ref 20, 21).

Zeumer et al. found that the appropriate addition of Ta could increase the high-temperature strength of NiAl alloy by two times due to the presence of Laves phases (Ref 22). Inspired by this, Sheng et al. prepared NiAl-Cr(Mo)-Ta eutectic alloy, whose microstructure was composed of primary NiAl phase, NiAl + Cr(Mo) eutectic and a little Cr_2Ta phase and the high-temperature strength of alloy improved (Ref 18). In addition, studies have shown that adding Ta to NiAl and Ni-based superalloys can effectively improve the high-temperature oxidation resistance (Ref 23-25). In the NiAl-Cr(Mo) alloy,

Zhao Shang, Tian Liu, Wenfang Bai, Xiaowan Dong, and **Jungang Yang**, School of Materials Science and Engineering, Xi'an University of Technology, Xi'an 710048, China; and **Jun Shen**, State Key Laboratory of Solidification Processing, Northwestern Polytechnical University, Xi'an 710072, China. Contact e-mails: shangzhao@xaut.edu.cn and yang-j-g@xaut.edu.cn.

Published online: 23 August 2024

the excellent oxidation resistance of NiAl alloy would be compromised by the addition of Mo (Ref 26, 27). So Ta addition may also improve the oxidation resistance of NiAl-Cr(Mo) alloy. Moreover, Cr(Mo) strengthening phase with large volume fraction can further improve the strength and fracture toughness in the NiAl-Cr(Mo) hypereutectic alloy (Ref 12). Therefore, different contents of Ta were added into the NiAl-32Cr-6Mo hypereutectic alloy in this work, hoping to obtain superior comprehensive properties so that it could meet the actual industrial requirements. The effects of Ta addition on the microstructure, compression properties at room temperature and 1000 °C, fracture behavior as well as oxidation resistance of alloy were investigated.

2. Experiments

NiAl-32Cr-6Mo-xTa (x = 0, 4, 6 and 8 at.%) alloy ingots were prepared using high-purity raw materials in a vacuum non-consumable arc melting furnace. Each alloy ingot was remelted 4-5 times to obtain uniform composition. The actual compositions of ingots tested by inductively coupled plasma technology (ICP) were Ni-30.9Al-32.1Cr-6.1Mo, Ni-29.1Al-32.1Cr-6Mo-3.9Ta, Ni-27.9Al-32.1Cr-5.9Mo-6.1Ta and Ni-26.9Al-32Cr-5.9Mo-8.1Ta, respectively, which were in agreement with the designed compositions, so the nominal compositions were used below. The samples for microstructure observation, mechanical test and isothermal oxidation were cut from the alloy ingots by electrical discharge machining (EDM). After grinding and polishing, the metallographic samples were etched with a solution of 75% HCl + 25% HNO_3 by volume. Scanning electron microscope (SEM) was used to examine the microstructures, while x-ray diffraction (XRD, Cu Kα target) and energy-dispersive spectroscopy (EDS) were used to identify phase constitution. The volume fraction of each phase in the alloys was measured by Image Pro Plus 6.0 software, ten SEM pictures were used for each measurement, and the average value was employed.

The mechanical samples with a size of φ4 × 7 mm were compressed at room temperature and 1000 °C, respectively. The HT-2402 material testing machine was utilized to conduct room-temperature compression test at a strain rate of 2×10^{-3} s^{-1}. The Gleeble 3500 heat/force modeling test machine was used to conduct high-temperature compression test at a vacuum of 1×10^{-2} Pa and a strain rate of 4.2×10^{-4} s^{-1}. When the true compression strain reached 35%, the high-temperature compression test was terminated. The fracture morphologies and compression microstructures of alloys were observed by SEM. The samples with a size of φ4 × 4 mm for isothermal oxidation were placed in a LSL-1700X high-temperature furnace at 1000, 1050 and 1100 °C, respectively. For the four alloys, the starting weights are 0.308, 0.342, 0.360 and 0.377 g, respectively. At temperatures below 1000 °C, the heating rate was 10 °C/min; if the temperature exceeded 1000 °C, the rate decreases to 5 °C/min to reach the desired temperature. When the samples were oxidized for 1, 4, 8, 16 and 24 h, respectively, they were taken out and weighed by a Mettler's UMT2 electronic balance with an accuracy of 10^{-4} g. The static weight gain method was used to obtain the mass change versus oxidation time of alloys. In order to ensure the reliability, three samples were used for the compression and oxidation under each condition, and then, the average value was taken as the final test result.

3. Results and Discussion

3.1 Phase Constitution

From the XRD patterns of NiAl-32Cr-6Mo-xTa (x = 0, 4, 6 and 8 at.%) alloys shown in Fig. 1, the microstructures of all alloys contain two phases of NiAl and Cr, and the diffraction peak of Cr_2Ta could be observed after the addition of Ta. The similar result was also obtained by Sheng et al. in the cast NiAl-Cr(Mo)-Ta eutectic alloy (Ref 18). However, the position of Cr peak shifted significantly to the left, which may be due to the solution of other atoms in the multi-component alloys.

3.2 Microstructures

Figure 2 shows the microstructures of NiAl-32Cr-6Mo-xTa (x = 0, 4, 6 and 8 at.%) alloys. The NiAl-32Cr-6Mo alloy with no Ta addition is only composed of gray and dark phases. After adding Ta element, white phase is formed. In Fig. 2(a) and (b), primary dendrites with irregularly chrysanthemum eutectic cells are observed. Through XRD result in Fig. 1, EDS result in Table 1 and previous researches (Ref 12, 28), the dark phase is NiAl and the gray phase is Cr(Mo), respectively. Therefore, each eutectic cell is composed of alternating NiAl and Cr(Mo) two-phase lamellae. The Cr(Mo) phase mentioned in the paper is actually a Cr phase with a large number of Mo atoms solidly dissolved. Many similar results were found in the previous studies (Ref 11, 17, 29, 30). In addition, the atomic radius of Mo is larger than that of Cr, which will increase the lattice constant of Cr phase, so the diffraction peak of the Cr phase in Fig. 1 shifts to the left compared with the standard diffraction peak of the Cr phase.

From Fig. 2(c) and (d), not only the primary Cr(Mo) phase, but also the darker cellular regions and the bright irregular regions are observed. The size of eutectic cell becomes smaller, and the shape becomes more irregular. According to the EDS result in Table 1, Cr, Mo, Ni, Al and Ta exist in the white phase, and the atomic percentage ratio of Cr and Ta is close to 2:1. Combined with previous studies (Ref 18, 31), the Cr_2Ta phase with C_{14} crystal structure is formed and it mainly distributed at the cell boundary. In addition, Ta could be dissolved into the dark phase, gray phase and white phase, but the content in white phase is the largest. Significantly, from the high magnification microstructure in Fig. 2(d), the darker cellular regions are composed of two-phase lamellae of NiAl and Cr(Mo), while the brighter irregular regions are composed of NiAl, Cr(Mo) and Cr_2Ta three-phase lamellae. Therefore, NiAl + Cr(Mo) two-phase eutectic and NiAl + Cr(Mo) + Cr_2Ta three-phase eutectic exist together in the NiAl-Cr(Mo)-Ta alloy.

In Fig. 2(e) and (f), both primary Cr(Mo) and Cr_2Ta dendrites appear. Compared with NiAl-32Cr-6Mo-4Ta alloy, the content of massive Cr_2Ta decreases due to the appearance of primary Cr_2Ta dendrites, indicating that the Cr_2Ta phase mainly exists as Cr_2Ta dendrites. When Ta content is 8 at.%, the number of primary Cr_2Ta dendrites increases significantly, and no primary Cr(Mo) dendrites exit, the primary phase wholly changes from Cr(Mo) to Cr_2Ta. The darker NiAl + Cr(Mo) two-phase eutectic is more likely to appear around the primary

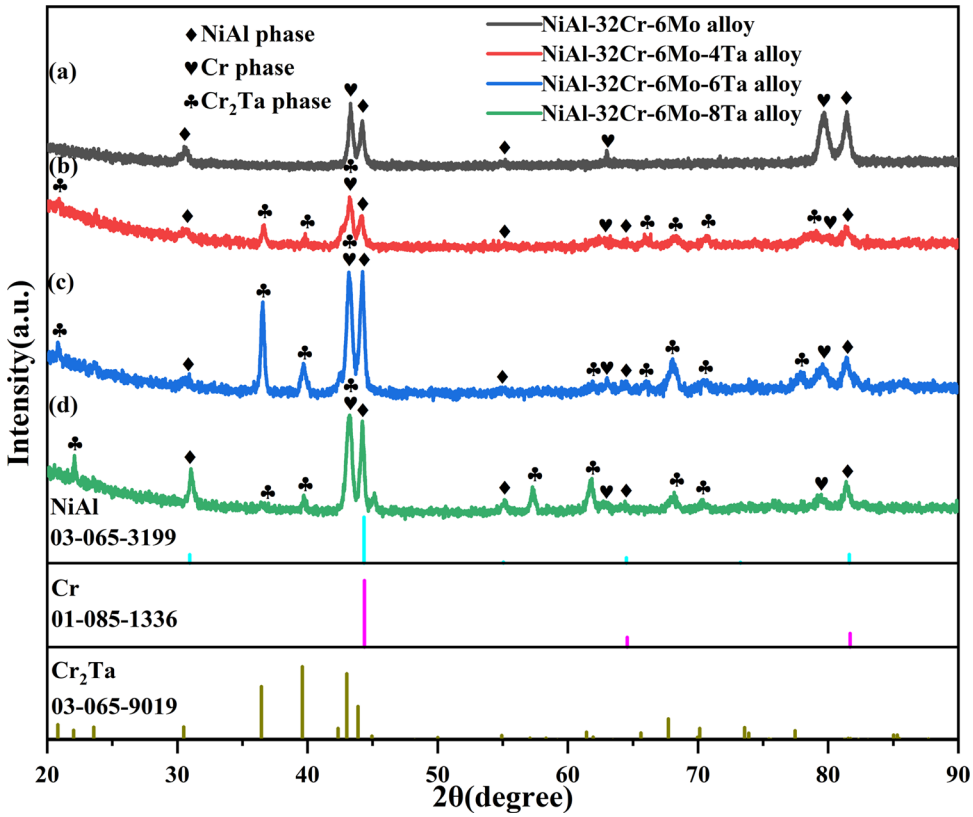

Fig. 1 XRD patterns of the NiAl-32Cr-6Mo-xTa alloys: (a) x = 0; (b) x = 4; (c) x = 6; (d) x = 8 at.%, respectively

Cr_2Ta dendrites. In the previous work of Sheng et al. (Ref 18), only NiAl + Cr(Mo) two-phase eutectic was observed, and no Cr_2Ta primary dendrites appeared. The significant differences may be related to the composition of the alloy, which is hypereutectic in this work.

The composition of NiAl-32Cr-6Mo alloy locates in the range of hypereutectic, and some Cr(Mo) primary dendrites appear. Table 2 shows volume fractions (%) of component phases and primary dendrites in the NiAl-32Cr-6Mo-xTa (x = 0, 4, 6 and 8 at.%) alloys. Since the melting point of Cr_2Ta phase (2020 °C) is obviously higher than Cr(Mo) phase (1820 °C), the Cr_2Ta phase is preferentially formed during solidification. The content of Ta in the NiAl-32Cr-6Mo-4Ta alloy is relatively low, and there is only a small amount of Cr_2Ta phase in the microstructure, which is not enough to produce Cr_2Ta dendrites. With the increasing Ta content, Cr_2Ta dendrites appear and Cr(Mo) dendrites gradually decrease. When Ta content is 8%, Cr(Mo) dendrites totally disappear, and all primary dendrites are Cr_2Ta (about 12.5%).

3.3 Room-Temperature Compression Properties

Figure 3 and Table 3 show the engineering stress–strain curves and detailed values of room-temperature compression properties of NiAl-32Cr-6Mo-xTa (x = 0, 4, 6 and 8 at.%) alloys, respectively. When the stress reaches the maximum, the fracture will occur, showing typical brittle fracture characteristics. The compression strength and strain of as-cast NiAl alloy are 562 MPa and 6.3%, respectively (Ref 32). In the NiAl-32Cr-6Mo alloy, they dramatically increase to 2108.7 MPa and 18.7%, respectively, which proves that the Cr(Mo) strengthening phase has a positive effect on the strength and ductility of alloy. When 4 and 6 at.% Ta are added to the alloys, the compression strengths reduce to 1531.5 and 1538.0 MPa, respectively. These values are a little higher than those of NiAl-32Cr-6Mo-1Ti (about 1432 MPa) and NiAl-32Cr-6Mo-3Nb (about 1473 MPa) alloys in our previous studies (Ref 17, 33). Generally, precipitation strengthening and solution strengthening are beneficial to the improvement of strength, but cracks preferentially propagate along the boundary of eutectic cell and the interface between the primary phase and the eutectic in the off-eutectic composition alloy, which greatly reduces the compression strength of alloys (Ref 12, 34, 35). When the Ta content further increases to 8 at.%, the compression strength continually decreases to 1326 MPa. In addition, the compression strain of alloys also obviously decreases after Ta addition. Of course, the rapidly expanding crack inevitably leads to the decrease in the plasticity of the alloy. Furthermore, as intermetallics, Cr_2Ta phase is hard and brittle, its increasing volume fraction also decreases the plasticity of Ta-containing alloys. Overall speaking, the NiAl-32Cr-6Mo-6Ta has better mechanical properties in the above Ta-containing alloys.

3.4 High-Temperature Compression Properties

The high-temperature compression result of NiAl-32Cr-6Mo-xTa (x = 0, 4, 6 and 8 at.%) alloys is displayed in Table 4. The compression strength of binary NiAl alloy is only 55 MPa at 1000 °C (Ref 36) and that of NiAl-32Cr-6Mo alloy is 247.6 MPa at 1000 °C in this work. Through adding 4 at.% Ta, the compression strength considerably increases to 474.2 MPa. When 6 at.% Ta is added, the compression strength is 475.1 MPa, which is about nine times than that of binary NiAl alloy and two times than that of NiAl-32Cr-6Mo alloy. Both the

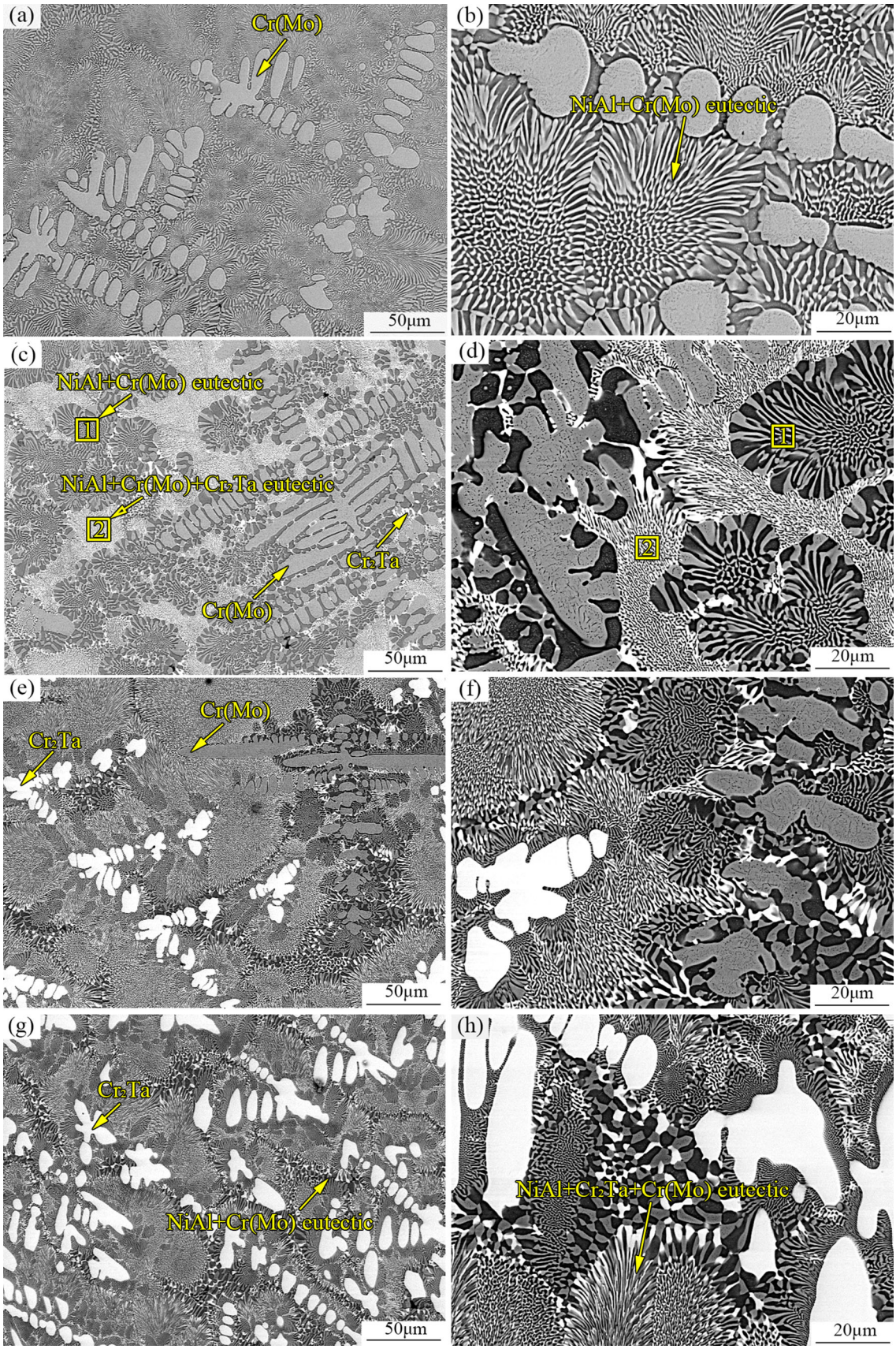

Fig. 2 Microstructure of the NiAl-32Cr-6Mo-xTa alloys: (a), (b) x = 0; (c), (d) x = 4; (e), (f) x = 6; (g), (h) x = 8 at.%, respectively

Table 1 Compositions of the constituent phases in the NiAl-32Cr-6Mo and NiAl-32Cr-6Mo-4Ta alloys by EDS test

Alloys	Phase	Ni	Al	Cr	Mo	Ta
NiAl-32Cr-6Mo	Dark phase	45.84	42.06	11.48	0.62	…
	Gray phase	12.72	8.84	62.70	15.74	…
NiAl-32Cr-6Mo-4Ta	Dark phase	49.52	41.38	7.80	0.38	0.92
	Gray phase	6.28	11.74	64.47	13.48	4.03
	White phase	14.13	6.52	47.99	6.75	24.61

Table 2 Volume fractions (%) of component phases and primary dendrites in the NiAl-32Cr-6Mo-xTa (x = 0, 4, 6 and 8 at.%) alloys

Alloys	NiAl phase	Cr(Mo) phase	Cr_2Ta phase	Cr(Mo) dendrites	Cr_2Ta dendrites
NiAl-32Cr-6Mo	48.3	51.7	…	13.4	…
NiAl-32Cr-6Mo-4Ta	49.4	44.1	6.5	10.9	…
NiAl-32Cr-6Mo-6Ta	50.2	39.5	10.3	5.5	7.5
NiAl-32Cr-6Mo-8Ta	52.4	32.9	14.7	…	12.5

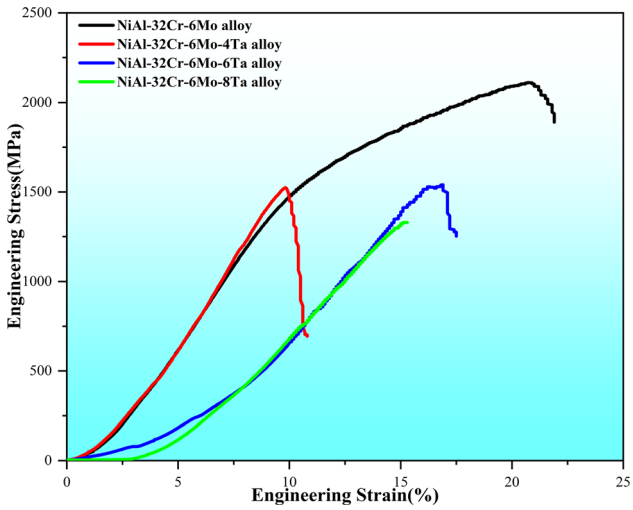

Fig. 3 Room-temperature compression engineering stress–strain curves of the NiAl-32Cr-6Mo-xTa (x = 0, 4, 6 and 8 at.%) alloys

Table 3 Room-temperature compression properties of the NiAl-32Cr-6Mo-xTa (x = 0, 4, 6 and 8 at.%) alloys

Alloys	Compression strength, MPa	Compression strain, %
NiAl-32Cr-6Mo	2108.7 ± 31.1	18.7 ± 0.8
NiAl-32Cr-6Mo-4Ta	1531.5 ± 20.0	10.4 ± 2.1
NiAl-32Cr-6Mo-6Ta	1538.0 ± 25.3	15.2 ± 1.5
NiAl-32Cr-6Mo-8Ta	1326.0 ± 24.4	15.2 ± 2.3

Table 4 High-temperature compression strength of the NiAl-32Cr-6Mo-xTa (x = 0, 4, 6 and 8 at.%) alloys

Alloys	Compression strength (MPa)
NiAl-32Cr-6Mo	247.6 ± 4.6
NiAl-32Cr-6Mo-4Ta	474.2 ± 3.6
NiAl-32Cr-6Mo-6Ta	475.1 ± 4.9
NiAl-32Cr-6Mo-8Ta	472.2 ± 5.1

values are higher than that of NiAl-32Cr-6Mo-1Nb (about 424 MPa at 1000 °C) alloy (Ref 37). More importantly, the NiAl-Cr(Mo)-Hf alloy, which is regarded as a traditional high strength alloy, has a compression strength of 430 MPa at 1000 °C (Ref 38). The addition of Ta is also better than that of Nb and Hf for the promotion of high-temperature strength of NiAl-Cr(Mo) alloy. After adding 8 at.%Ta, the compression strength is 472.2 MPa. In addition, the high-temperature compression engineering stress–strain curves of NiAl-32Cr-6Mo-xTa (x = 0, 4, 6 and 8 at.%) alloys are shown in Fig. 4. All alloys at high temperature show plastic fracture. It is worth noting that the high-temperature compression strength of NiAl-32Cr-6Mo-8Ta alloy is slightly below and the compression strain is obviously below than that of 4Ta and 6Ta alloys; meanwhile, the stress–strain curve of NiAl-32Cr-6Mo-8Ta alloy drops rapidly and its decline rate is also greater than 4Ta and 6Ta alloys. In the NiAl-32Cr-6Mo-8Ta alloy, many brittle Cr_2Ta dendrites appear, leading to the lower compression strength and strain both at room temperature and high temperature. From the above results, it could be concluded that the upper limit of Ta addition should not exceed 8%.

3.5 Fracture Morphologies and Strengthening Mechanism

To study the fracture behaviors of NiAl-32Cr-6Mo-xTa (x = 0, 4, 6 and 8 at.%) alloys, the fracture morphologies after

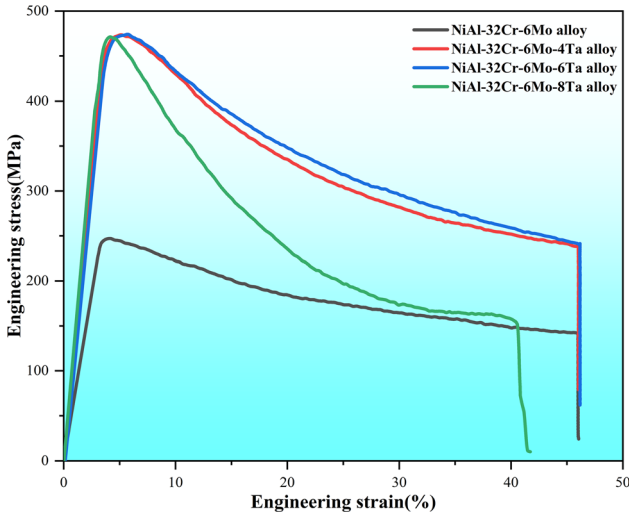

Fig. 4 High-temperature compression engineering stress–strain curves of the NiAl-32Cr-6Mo-xTa (x = 0, 4, 6 and 8 at.%) alloys

room-temperature compression are shown in Fig. 5. Although the fractures of all alloys show the characteristics of brittle pseudo-cleavage fractures, the macroscopical fracture morphologies are different. The fluvial cleavage planes and uneven tearing ridges as well as some dark primary Cr(Mo) dendrites are observed in the fracture of NiAl-32Cr-6Mo alloy. From the disordered cleavage fracture of two-phase eutectic lamellae, great resistance is subjected during the fracture process, meaning the higher compression strength. The strength of Cr(Mo) phase is significantly greater than NiAl phase (Ref 12), which is conducive to improving the compression strength of alloy.

From Fig. 5(c), (d), (e), (f), (g) and (h), the fracture surfaces of the Ta-containing alloys are relatively flat. Fewer cleavage steps and tearing ridges are observed, indicating that there is no large resistance to prevent crack propagation during the fracture process, so the compression strength is relatively lower. In addition, many primary dendrites are observed, whether Cr(Mo) or Cr_2Ta dendrites. The fracture surface of primary dendrites is very smooth, and the deformation is very small when the force loading is applied. Although the Cr(Mo) and Cr_2Ta phases have high strengths, the crack always extends along the eutectic cell boundary and the interface between the primary phase and the eutectic (Ref 34, 39), as shown in Fig. 6, resulting in a lower compression strength than the NiAl-32Cr-6Mo alloy. The result is also consistent with compression stress–strain curves at room temperature.

From the above results, Ta addition significantly affects the room-temperature compression properties due to the variations of microstructure and volume fraction of primary dendrites. The compression strength of NiAl-32Cr-6Mo alloy is much higher than the binary NiAl alloy due to the positive effect by Cr(Mo) strengthening phase. Obviously, the solution strengthening of Ta and the precipitation strengthening of Cr_2Ta phase are advantageous for the enhancement of strength. But the volume fraction of the primary dendrites increases with the increasing Ta content for non-eutectic alloys, and cracks are easy to extend along the interface between primary dendrites and eutectic. Furthermore, the addition of Ta also makes the eutectic microstructure become irregular, which is also adverse for the room-temperature compression strength. In a word, the effect of weakening is greater than strengthening in the Ta-containing alloys, so the compression strength is lower than that of NiAl-32Cr-6Mo alloy at room temperature. Of course, for directionally solidified alloys, regular eutectic lamellae with a large volume fraction can also be obtained under hypereutectic composition due to the high-temperature gradient (Ref 40). Therefore, Cr(Mo) and Cr_2Ta strengthening phases may be able to enhance the properties of directionally solidified hypereutectic alloys, which will be further investigated in future.

The microstructures of NiAl-32Cr-6Mo-xTa (x = 0, 4, 6 and 8 at.%) alloys after high-temperature compression are shown in Fig. 7. From Fig. 7(a), the cracks in NiAl-32Cr-6Mo alloy are generated and propagated along the boundary of eutectic cells after high-temperature compression, which implies the binding strength of boundary is low (Ref 39). However, the cracks in NiAl-32Cr-6Mo-6Ta and NiAl-32Cr-6Mo-8Ta alloys all pass through the primary Cr_2Ta phase from Fig. 7(c) and (d), which is due to the stress concentration leading to the cracking of the hard and brittle Cr_2Ta phase. This phenomenon also appears in Cr-Cr_2Ta alloys studied by Bhowmik et al. (Ref 41). It is noteworthy that crack propagation along the interface of primary phase and eutectic is not observed in the Ta-containing alloys. Cracks propagate intracellularly after high-temperature compression due to the Cr_2Ta + NiAl + Cr(Mo) three-phase eutectic along the cell boundary in the Ta-containing alloys, as shown in Fig. 8, indicating that these interfaces are no longer weak. Overall, the precipitation strengthening of Cr_2Ta, solid solution strengthening of Ta and the strong interface all contribute to the improved high-temperature strength of Ta-containing alloys.

3.6 Isothermal Oxidation

Figure 9 shows the mass change vs. oxidation time of NiAl-32Cr-6Mo-xTa (x = 0, 4, 6 and 8 at.%) alloys after isothermal oxidation for 24 h at 1000, 1050 and 1100 °C. The mass changes of four alloys increase with the increasing time and reach 0.22, 0.16, 0.17 and 0.17 mg after oxidation at 1000 °C for 24 h. With the increasing oxidation temperature, the Ta-containing alloys have a significantly decreased mass change compared with NiAl-32Cr-6Mo alloy. Particularly, the mass change of NiAl-32Cr-6Mo-4Ta alloy is 0.54 mg cm^{-2} at 1100 °C for 24 h, which is about one-third of that of NiAl-32Cr-6Mo alloy. On the whole, the mass change of Ta-containing alloy is obviously smaller than that of NiAl-32Cr-6Mo alloy at all temperatures, which indicates that the oxidation rate of alloy can be reduced by Ta addition. Gao et al. found that Ta element could hinder the internal diffusion of O^{2-} and the external diffusion of Al^{3+}, avoid excessive consumption of Al and promote the formation of Al_2O_3 oxide film protective film (Ref 42, 43), thus leading to the excellent oxidation resistance of NiAl-Cr(Mo)-Ta alloys. In addition, as the temperature further increases, the differences in the mass change between the NiAl-32Cr-6Mo alloy and NiAl-32Cr-6Mo-xTa (x = 4 and 6) become larger, meaning selecting an appropriate addition amount is also important and Ta has a more significant effect on the oxidation resistance at higher temperature, which would be further studied in the following work.

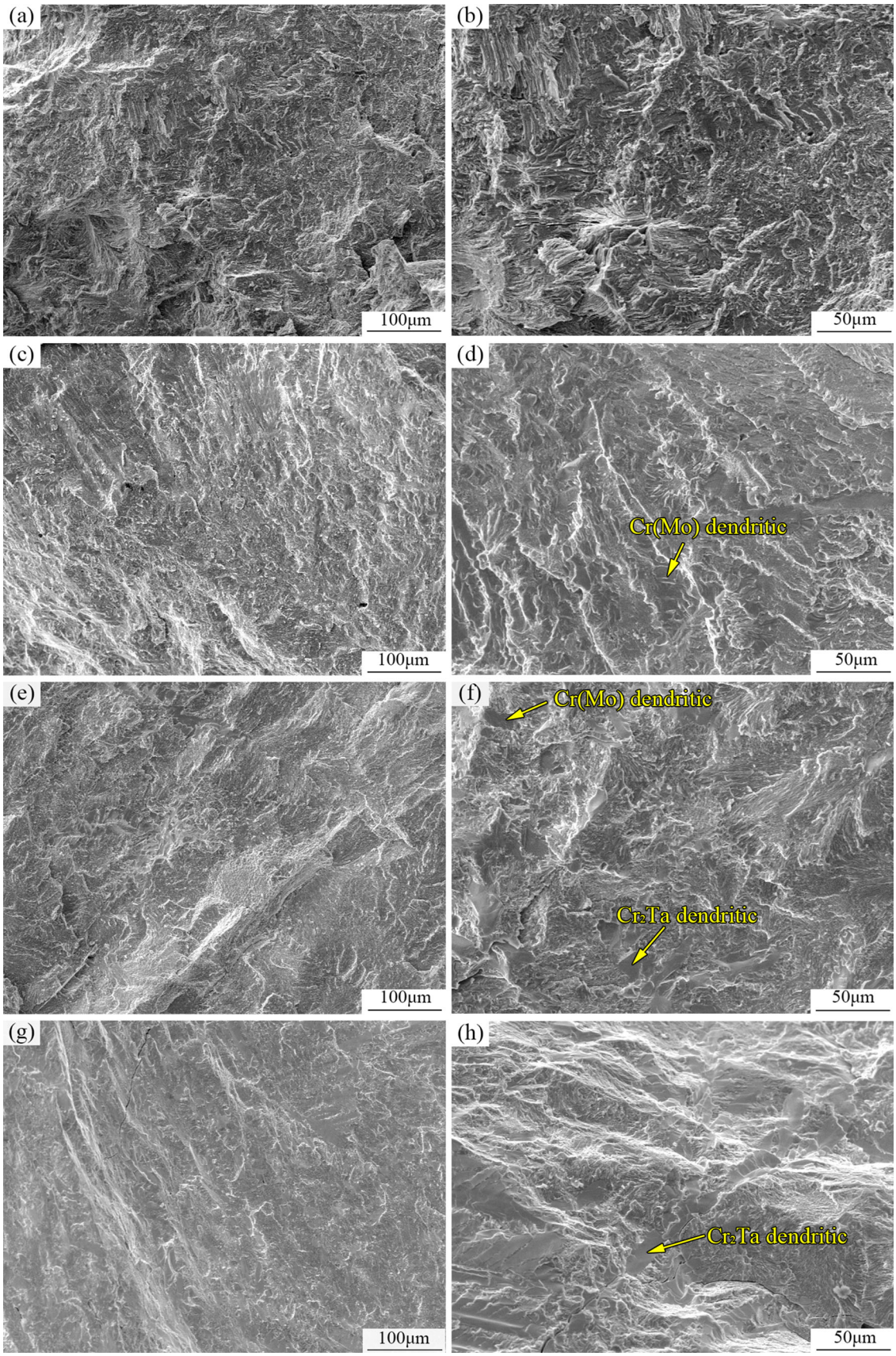

Fig. 5 Fracture morphologies of the NiAl-32Cr-6Mo-xTa alloys after room-temperature compression: (a), (b) $x = 0$; (c), (d) $x = 4$; (e), (f) $x = 6$; (g), (h) $x = 8$ at.%, respectively

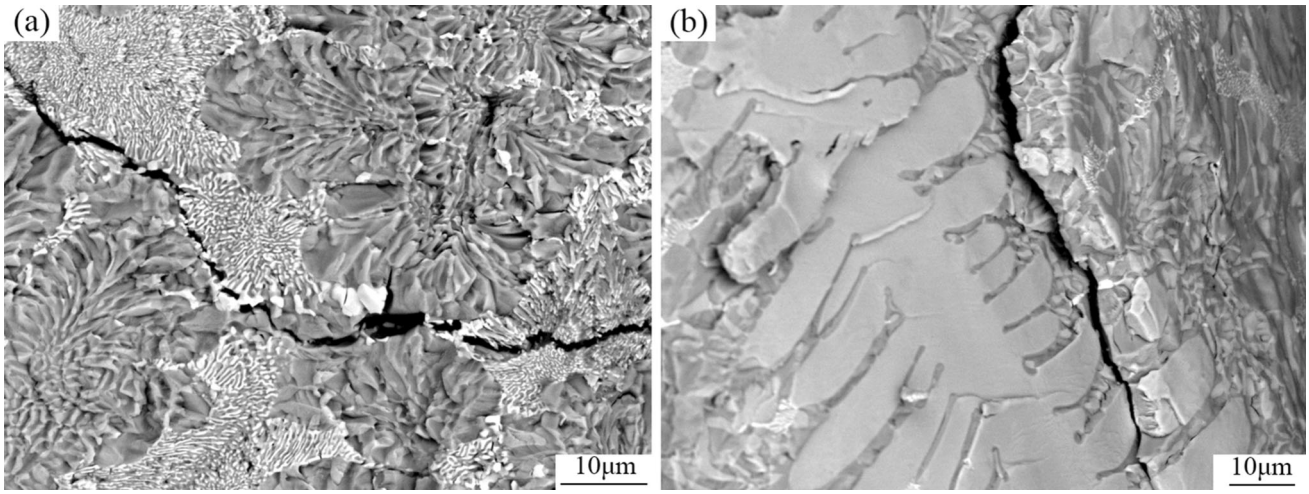

Fig. 6 Crack propagation of the NiAl-32Cr-6Mo-4Ta alloy after room-temperature compression

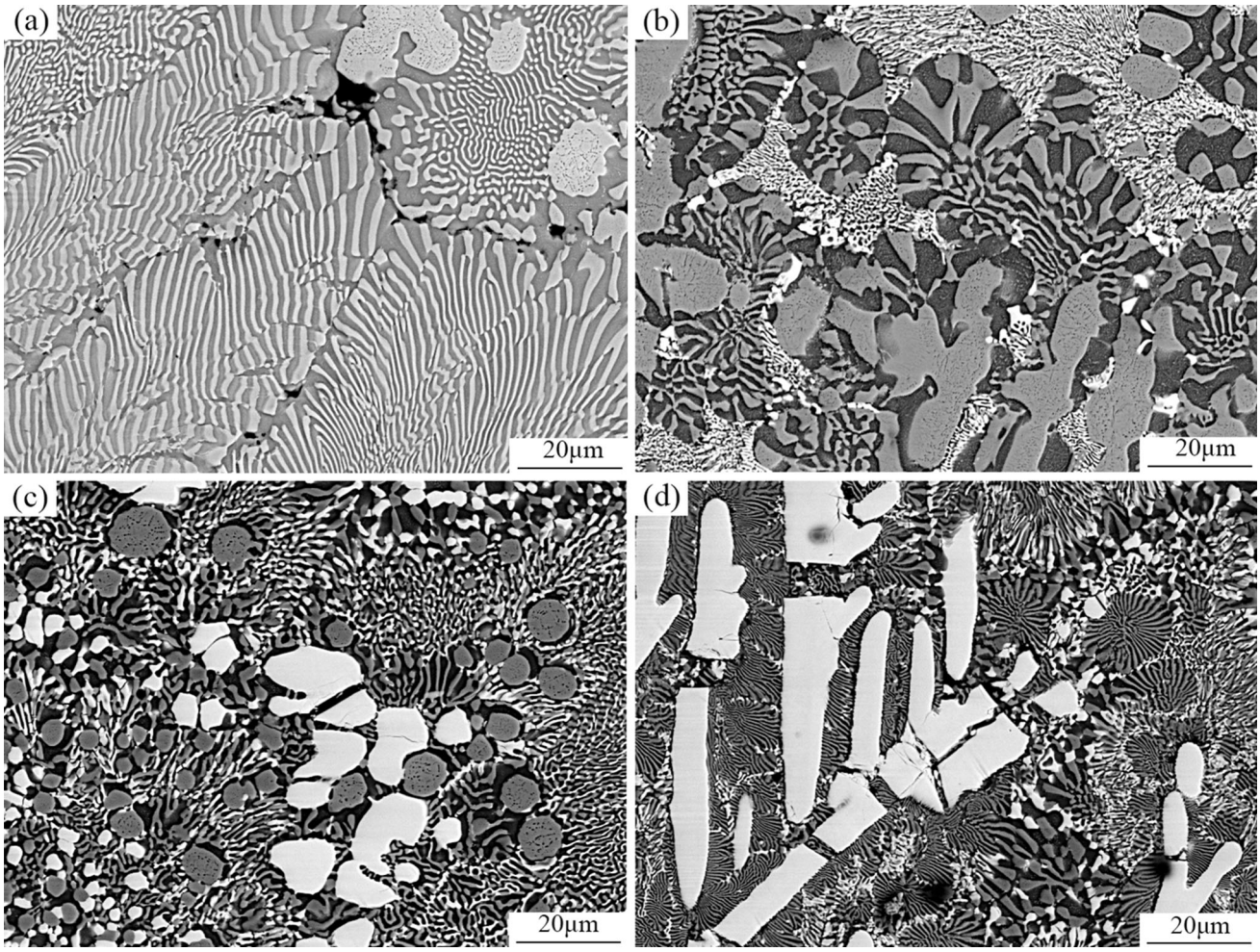

Fig. 7 Microstructures of the NiAl-32Cr-6Mo-xTa alloys after high-temperature compression: (a) $x = 0$; (b) $x = 4$; (c) $x = 6$; (d) $x = 8$ at.%, respectively

4. Conclusion

1. The microstructure of NiAl-32Cr-6Mo alloy comprises NiAl + Cr(Mo) eutectic cells and primary Cr(Mo) dendrites, and Ta addition leads to the formation of Cr_2Ta phase. With the increasing Ta, the primary phase changes from Cr(Mo) to Cr_2Ta. Both NiAl + Cr(Mo) two-phase eutectic and NiAl + Cr(Mo) + Cr_2Ta three-phase eutectic are observed in Ta-containing alloys.

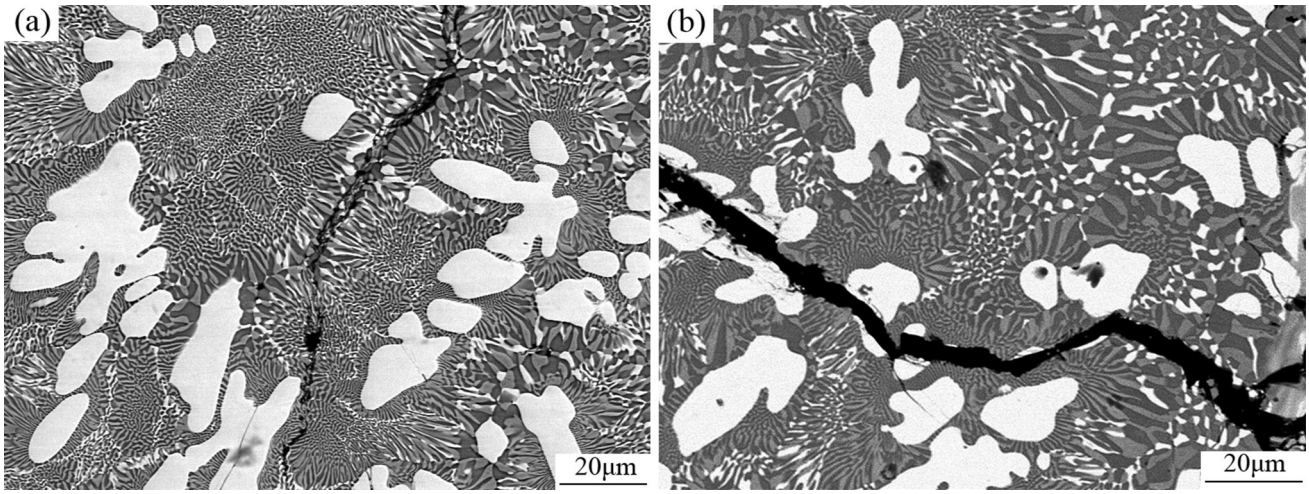

Fig. 8 Crack propagation in the NiAl-32Cr-6Mo-8Ta alloy after high-temperature compression

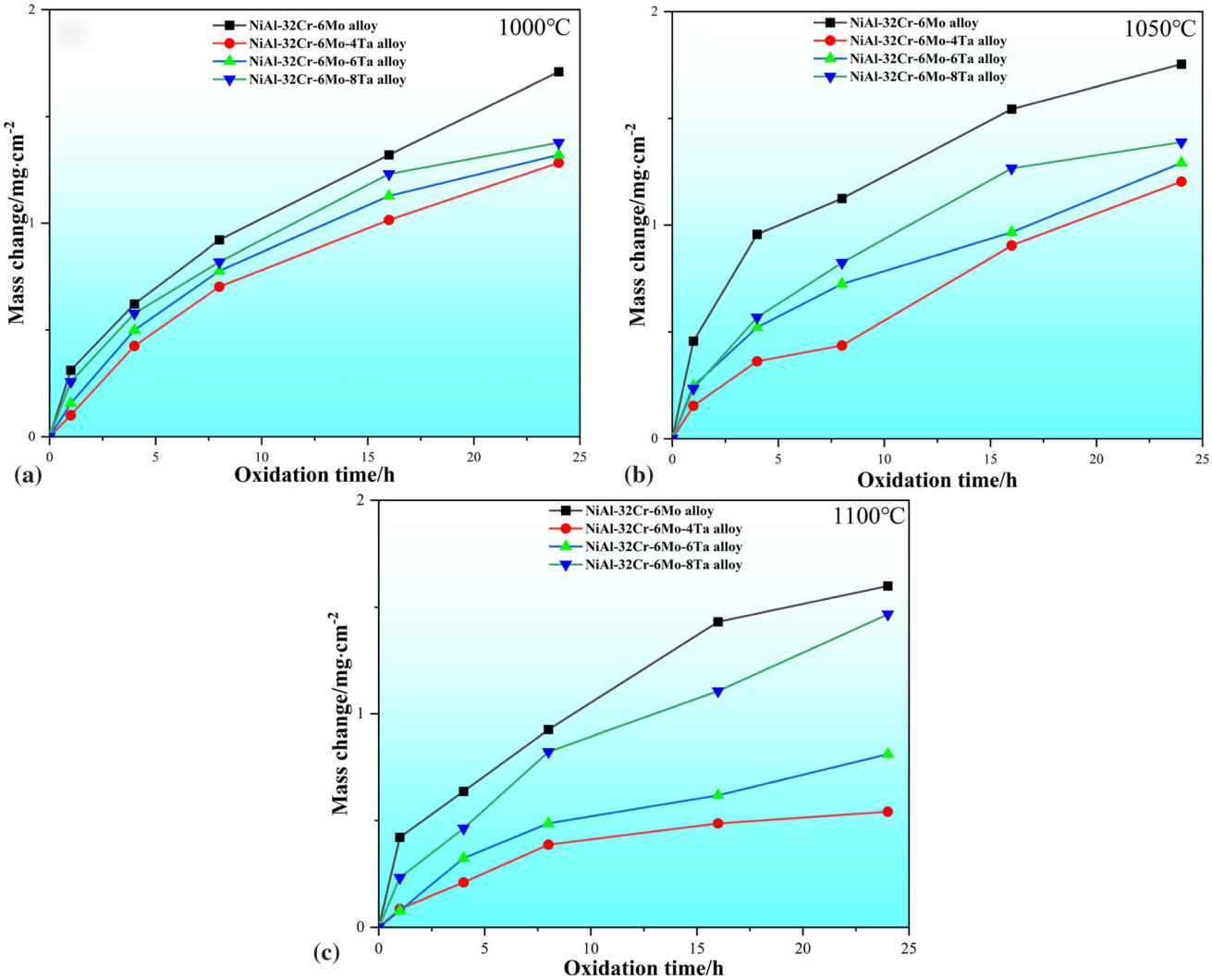

Fig. 9 Mass change vs. oxidation time of NiAl-32Cr-6Mo-xTa (x = 0, 4, 6 and 8 at.%) alloys at different temperatures: (a)1000; (b) 1050; (c) 1100 °C

2. After adding Ta, the room-temperature compression strength decreases, while the high-temperature compression strength significantly increases. The compression strength of NiAl-32Cr-6Mo-6Ta alloy is 475.1 MPa at 1000 °C, which is about 9 times than that of binary NiAl alloy and 2 times than that of NiAl-32Cr-6Mo alloy.
3. All alloys show brittle pseudo-cleavage fractures at room temperature. The volume fraction of the primary dendrites increases with the increasing Ta content, and cracks tend to extend along the interface between primary dendrites and eutectic. Furthermore, Ta addition also makes the eutectic microstructure become irregular. The above two factors make the room-temperature compression strength of all Ta-containing alloys lower than that of NiAl-32Cr-6Mo alloy.
4. At 1000 °C, all alloys show plastic fracture. Crack propagation along the boundary of primary phase and eutectic is not observed in the Ta-containing alloys, indicating that these interfaces are no longer weak at high temperature. The precipitation strengthening of Cr_2Ta, solid solution strengthening of Ta and the strong interface all contribute to the improved high-temperature strength of Ta-containing alloys.
5. The mass change of Ta-containing alloy after oxidation is smaller than that of NiAl-32Cr-6Mo alloy at all temperatures, and Ta addition could obviously increase the oxidation resistance of alloy. In addition, selecting an appropriate addition amount is also important and Ta has a more significant effect on the oxidation resistance at higher temperature.

Acknowledgments

The authors gratefully acknowledge the Natural Science Basic Research Plan in Shaanxi Province of China (No. 2024JC-YBMS-411) and Shaanxi Province Qinchuangyuan ‘‘scientist + engineer’’ team construction project (No. 2024QCY-KXJ-115).

Conflict of interest

On behalf of all authors, the corresponding author states that there is no conflict of interest.

References

1. N.K. Adomako, N. Haghdadi, and S. Primig, Electron and Laser-Based Additive Manufacturing of Ni-Based Superalloys: A Review of Heterogeneities in Microstructure and Mechanical Properties, *Mater. Des.*, 2022, **223**, p 111245
2. W. Liu, S. Huang, C.T. Ye, L. Jia, Y.W. Kang, J.B. Sha, B.Q. Chen, Y. Wu, and H.P. Xiong, Progress in Nb-Si Ultra-High Temperature Structural Materials: A Review, *J. Mater. Sci. Technol.*, 2023, **149**, p 127–153
3. Y.Z. Wei, L.Y. Zhao, L.H. Shi, H.Y. Yang, R.F. Guo, H.L. Zhao, L.Y. Chen, F. Qiu, Q.C. Jiang, and L.C. Zhang, Excellent Strength-Toughness Combination of NiAl-30Cr Composites with Novel In Situ Composite Microstructure Containing NiAl Matrix and Cr Single-Phase, *Mater. Sci. Eng. A*, 2024, **897**, p 146341
4. Z. Shang, Q.W. Zhang, J. Shen, H.Q. Bai, H.L. Liang, L.S. Zhong, and Y.H. Xu, Effects of V Addition on the Solidification Microstructures and Room Temperature Compression Properties of NiAl-Cr(Mo) Hypereutectic Alloy, *Vacuum*, 2020, **179**, p 109507
5. K. Bochenek and M. Basista, Advances in Processing of NiAl Intermetallic Alloys and Composites for High Temperature Aerospace Applications, *Prog. Aerosp. Sci.*, 2015, **79**, p 136–146
6. B. Li, H.J. Guo, C. Li, Y.M. Gao, Y.Z. Shi, Z.Y. Pei, S.J. Wang, and C.Y. Liang, The Microstructure Characteristics and Self-Lubrication Mechanism of the NiAl Matrix Composites Prepared by Vacuum Hot-Pressing Sintering, *Vacuum*, 2022, **205**, p 111488
7. T.W.B. Riyadi, T. Zhang, D. Marchant, and X.M. Zhu, NiAl-TiC-Al_2O_3 Composite Formed by Self-Propagation High-Temperature Synthesis Process: Combustion Behaviour, Microstructure, and Properties, *J. Alloys Compd.*, 2019, **805**, p 104–112
8. D.J. Wang, Y. Liang, H.W. Ning, and B. Wang, Effects of Zr and Co on the Microstructure and Mechanical Properties of NiAl-Based Alloys, *J. Alloys Compd.*, 2021, **883**, p 160815
9. Z. Shang, Q.W. Zhang, J. Shen, H.Q. Bai, X.W. Dong, W.F. Bai, L.S. Zhong, G. Liu, and Y.H. Xu, Effects of Nb/Ti Additions and Heat Treatment on the Microstructure Evolution and Hardness of As-Cast and Directionally Solidified NiAl-Cr(Mo) Alloy, *J. Mater. Res. Technol.*, 2021, **10**, p 905–915
10. Y.C. Zhu, S.C. Zhou, L. Wang, Y.J. Liang, Y.F. Xue, and L. Wang, Improving the Ductility of High-Strength Multiphase NiAl Alloys by Introducing Multiscale High-Entropy Phases and Martensitic Transformation, *Mater. Sci. Eng. A*, 2021, **808**, p 140949
11. H.W. Ning, D.J. Wang, B. Wang, and G. Liu, Investigations on the NiAl-Cr(Mo) Eutectic Alloy with Optimized Microstructure and Improved Room-Temperature Compressive Properties, *Mater. Sci. Eng. A*, 2021, **813**, p 141138
12. Z. Shang, J. Shen, L. Wang, Y.J. Du, Y.L. Xiong, and H.Z. Fu, Investigations on the Microstructure and Room Temperature Fracture Toughness of Directionally Solidified NiAl-Cr(Mo) Eutectic Alloy, *Intermetallics*, 2015, **57**, p 25–33
13. D.J. Wang, H.W. Ning, B. Wang, G. Liu, and S.J. Yuan, Fabrication of a NiAl-Cr(Mo) Eutectic Alloy with Network Microstructure for High-Temperature Strengthening, *Mater. Sci. Eng. A*, 2022, **835**, p 142628
14. C.Y. Cui, J.T. Guo, and H.Q. Ye, Effects of Hf Additions on High-Temperature Mechanical Properties of a Directionally Solidified NiAl/Cr(Mo) Eutectic Alloy, *J. Alloys Compd.*, 2008, **463**, p 263–270
15. J.T. Guo, L.Y. Sheng, Y.X. Tian, L.Z. Zhou, and H.Q. Ye, Effect of Ho on the Microstructure and Compressive Properties of NiAl-Based Eutectic Alloy, *Mater. Lett.*, 2008, **62**, p 3910–3912
16. K.W. Huai, J.T. Guo, Z.R. Ren, Q. Gao, and R. Yang, Effect of Nb on the Microstructure and Mechanical Properties of Cast NiAl-Cr (Mo) Eutectic Alloy, *J. Mater. Sci. Technol.*, 2006, **22**, p 164
17. Z. Shang, X.W. Dong, J. Shen, W.F. Bai, H.J. Niu, L. Gao, and L.S. Zhong, Effects of Ti Addition and Heat Treatment on the Microstructure and Mechanical Properties of NiAl-Cr(Mo) Hypereutectic Alloy, *J. Mater. Res. Technol.*, 2022, **20**, p 459–468
18. L.Y. Sheng, B.N. Du, C. Lai, J.T. Guo, and T.F. Xi, Influence of Tantalum Addition on Microstructure and Mechanical Properties of the NiAl-Based Eutectic Alloy, *Strength Mater.*, 2017, **49**, p 109–117
19. L. Wang and J. Shen, Effect of heat treatment on the microstructure and elevated temperature tensile property of Fe-doped NiAl-Cr(Mo)-(Hf, Dy) eutectic alloy, *Mater. Sci. Eng. A*, 2016, **654**, p 177–183
20. K.W. Huai, J.T. Guo, X.H. Du, and R. Yang, Microstructure and Mechanical Properties of NiAl-Cr(Mo)/Hf Alloy Prepared by Injection Casting, *Mater. Des.*, 2007, **28**, p 1940–1944
21. L.Y. Sheng, J.T. Guo, W.L. Ren, Z.X. Zhang, Z.M. Ren, and H.Q. Ye, Preliminary Investigation on Strong Magnetic Field Treated NiAl-Cr(Mo)-Hf Near Eutectic Alloy, *Intermetallics*, 2011, **19**, p 143–148
22. B. Zeumer and G. Sauthoff, Deformation Behaviour of Intermetallic NiAl Ta Alloys with Strengthening Laves Phase for High-Temperature Applications III. Effects of alloying with Cr, *Intermetallics*, 1998, **6**, p 451–460
23. H.B. Guo, D. Wang, H. Peng, S.K. Gong, and H.B. Xu, Effect of Sm, Gd, Yb, Sc and Nd as Reactive Elements on Oxidation Behaviour of β-NiAl at 1200 °C, *Corros. Sci.*, 2014, **78**, p 369–377
24. H.Z. Yang, J.P. Zou, Q. Shi, M.J. Dai, S.S. Lin, W. Du, and L. Lv, Analysis of the Microstructural Evolution and Interface Diffusion Behavior of NiCoCrAlYTa Coating in High Temperature Oxidation, *Corros. Sci.*, 2019, **153**, p 162–169
25. M. Yu, D.P. Zhou, J.B. Pu, T.C. Cui, and C.S. Li, Effect of Zr, Ti, Ta and Mo Addition on High-Temperature Oxidation and Hot Corrosion Behavior of NiAlY Alloys, *J. Alloys Compd.*, 2022, **908**, p 164614

26. B.H. Han, Y. Ma, H. Peng, L. Zheng, and H.B. Guo, Effect of Mo, Ta, and Re on High-Temperature Oxidation Behavior of Minor Hf Doped β-NiAl Alloy, *Corros. Sci.*, 2016, **102**, p 222–232
27. P.K. Ray, M. Akinc, and M.J. Kramer, Formation of Multilayered Scale during the Oxidation of NiAl-Mo Alloy, *Appl. Surf. Sci.*, 2014, **301**, p 107–111
28. L. Wang, C.L. Yao, J. Shen, Y.P. Zhang, T. Wang, H.X. Xu, L.H. Gao, and G.J. Zhang, Microstructures and Compressive Properties of NiAl-Cr(Mo) and NiAl-Cr Eutectic Alloys with Different Fe Contents, *Mater. Sci. Eng. A*, 2019, **744**, p 593–603
29. M. Khomutov, P. Potapkin, V. Cheverikin, P. Petrovskiy, A. Travyanov, I. Logachev, A. Sova, and I. Smurov, Effect of Hot Isostatic Pressing on Structure and Properties of Intermetallic NiAl-Cr-Mo Alloy Produced by Selective Laser Melting, *Intermetallics*, 2020, **120**, p 106766
30. L.F. Wei and Z.L. Zhao, Fabrication of the Lamellar NiAl Nanochannel by Selective Phase Dissolution of NiAl-Cr(Mo) Eutectic Alloy, *Corros. Sci.*, 2018, **138**, p 142–145
31. A. Bhowmik, K.M. Knowles, and H.J. Stone, Microstructural Evolution and Interfacial Crystallography in Cr-Cr2Ta, *Intermetallics*, 2012, **31**, p 34–47
32. L. Wang, J. Shen, Z. Shang, and H.Z. Fu, Microstructure Evolution and Enhancement of Fracture Toughness of NiAl-Cr(Mo)-(Hf, Dy) Alloy with a Small Addition of Fe during Heat Treatment, *Scr. Mater.*, 2014, **89**, p 1–4
33. Z. Shang, J. Shen, G. Liu, and Y.H. Xu, Investigations on the Solidification Microstructures and Room Temperature Compression Properties of Nb-Doped NiAl-32Cr-6Mo Hypereutectic alloy, *Mater. Sci. Eng., A*, 2018, **723**, p 89–96
34. L.Y. Sheng, J.T. Guo, Y.X. Tian, L.Z. Zhou, and H.Q. Ye, Microstructure and Mechanical Properties of Rapidly Solidified NiAl-Cr(Mo) Eutectic Alloy Doped with Trace Dy, *J. Alloys Compd.*, 2009, **475**, p 730–734
35. J.F. Zhang, J. Shen, Z. Shang, Z.R. Feng, L.S. Wang, and H.Z. Fu, Microstructure and Room Temperature Fracture Toughness of Directionally Solidified NiAl-Mo Eutectic In Situ Composites, *Intermetallics*, 2012, **21**, p 18–25
36. L.Y. Sheng, W. Zhang, J.T. Guo, F. Yang, Y.C. Liang, and H.Q. Ye, Effect of Au Addition on the Microstructure and Mechanical Properties of NiAl Intermetallic Compound, *Intermetallics*, 2010, **18**, p 740–744
37. L.Y. Sheng, J.T. Guo, and H.Q. Ye, Microstructure and Mechanical Properties of NiAl-Cr(Mo)/Nb Eutectic Alloy Prepared by Injection-Casting, *Mater. Des.*, 2009, **30**, p 964–969
38. L.Y. Sheng, L. Nan, W. Zhang, J.T. Guo, and H.Q. Ye, Microstructure and Mechanical Properties Determined in Compressive Tests of Quasi-Rapidly Solidified NiAl-Cr(Mo)-Hf Eutectic Alloy After Hot Isostatic Pressure and High Temperature Treatments, *J. Mater. Eng. Perform.*, 2010, **19**, p 732–736
39. L.Y. Sheng, F. Yang, T.F. Xi, Y.F. Zheng, and J.T. Guo, Microstructure and Room Temperature Mechanical Properties of NiAl-Cr(Mo)-(Hf, Dy) Hypoeutectic Alloy Prepared by Injection Casting, *Trans. N. Met. Soc. China*, 2013, **23**, p 983–990
40. Z. Shang, J. Shen, J. Zhang, L. Wang, and F. Hengzhi, Effect of Withdrawal Rate on the Microstructure of Directionally Solidified NiAl-Cr(Mo) Hypereutectic Alloy, *Intermetallics*, 2012, **22**, p 99–105. https://doi.org/10.1016/j.intermet.2011.10.018
41. A. Bhowmik, C.N. Jones, I.M. Edmonds, and H.J. Stone, Effect of Mo, Al and Si on the Microstructure and Mechanical Properties of Cr-Cr2Ta Based Alloys, *J. Alloys Compd.*, 2012, **530**, p 169–177
42. S. Gao, B. He, L.Z. Zhou, and J.S. Hou, Effects of Ta on the High Temperature Oxidation Behavior of IN617 Alloy in Air, *Corros. Sci.*, 2020, **170**, p 108682
43. C.T. Liu, J. Ma, X.F. Sun, and P.C. Zhao, Mechanism of the Oxidation and Degradation of the Aluminide Coating on the Nickel-Base Single-Crystal Superalloy DD32M, *Surf. Coat. Technol.*, 2010, **204**, p 3641–3646